Geochemistry Geophysics Geosystems G3

*Article*
Volume 13, Number 9
21 September 2012
Q09010, doi:10.1029/2012GC004304
ISSN: 1525-2027

Published by AGU and the Geochemical Society

# Controls of faulting and reaction kinetics on serpentinization and double Benioff zones

**Karthik Iyer and Lars H. Rüpke**
*The Future Ocean, GEOMAR, Helmholtz Centre for Ocean Research Kiel, Wischhofstraße 1-3, DE-24148 Kiel, Germany (kiyer@geomar.de)*

*SFB-574, GEOMAR, Helmholtz Centre for Ocean Research Kiel, Wischhofstraße 1-3, DE-24148 Kiel, Germany*

**Jason Phipps Morgan**
*Department of Earth and Atmospheric Sciences, Cornell University, Ithaca, New York 14853, USA*

**Ingo Grevemeyer**
*SFB-574, GEOMAR, Helmholtz Centre for Ocean Research Kiel, Wischhofstraße 1-3, DE-24148 Kiel, Germany*

[1] The subduction of partially serpentinized oceanic mantle may potentially be the key geologic process leading to the regassing of Earth's mantle and also has important consequences for subduction zone processes such as element cycling, slab deformation, and intermediate-depth seismicity. However, little is known about the quantity of water that is retained in the slab during mantle serpentinization and the pattern of serpentinization that may occur during bending-related faulting; an initial state that is essential for quantifying subsequent dehydration processes. We present a 2-D reactive-flow model simulating hydration processes in the presence of faulting at the trench outer-rise. We find that the temperature dependence of the serpentinization rate in conjunction with outer-rise faulting results in plate age and speed dependent patterns of hydration. Serpentinization also results in a reduction in surface heat flux toward the trench caused by advective downflow of seawater into the reaction region. Observed heat flow reductions are larger than the reduction due to the minimum-water downflow needed for partial serpentinization, predicting that active hydrothermal vents and chemosynthetic communities should also be associated with bend-fault serpentinization. Our model results agree with previous studies that the lower plane of double Benioff zones can be generated due to dehydration of serpentinized mantle at depth. More importantly, the depth-dependent pattern of serpentinization including reaction kinetics predicts a separation between the two Benioff planes consistent with seismic observations.

**Components:** 10,000 words, 9 figures.

**Keywords:** double seismic zones; numerical modeling; outer rise faulting; serpentinization; subduction; water cycle.

**Index Terms:** 0545 Computational Geophysics: Modeling (1952, 4255, 4316); 3017 Marine Geology and Geophysics: Hydrothermal systems (0450, 1034, 3616, 4832, 8135, 8424); 3060 Marine Geology and Geophysics: Subduction zone processes (1031, 3613, 8170, 8413).

**Received** 20 June 2012; **Revised** 22 August 2012; **Accepted** 22 August 2012; **Published** 21 September 2012.

Iyer, K., L. H. Rüpke, J. Phipps Morgan, and I. Grevemeyer (2012), Controls of faulting and reaction kinetics on serpentinization and double Benioff zones, *Geochem. Geophys. Geosyst.*, *13*, Q09010, doi:10.1029/2012GC004304.

## 1. Introduction

[2] Fluid flow and rock hydration at the trench outer-rise is a key process that influences subduction zone geodynamics as well as the water cycle. The presence of water and hydrated minerals in the downgoing slab reduces the strength of the incoming plate [*Escartín et al.*, 2001; *Karato and Wu*, 1993], influences element cycling [*Deschamps et al.*, 2011; *John et al.*, 2011; *Morris et al.*, 1990], triggers melting [*Ishikawa and Nakamura*, 1994; *Ulmer and Trommsdorff*, 1995] and deep seismicity [*Dobson et al.*, 2002; *Jung et al.*, 2004; *Peacock*, 2001], and may even be related to the evolution of the oceans [*Rüpke et al.*, 2004; *Wallmann*, 2001]. Therefore, constraining the distribution of water in the subducting lithosphere is critical to our understanding the past and present dynamics of the Earth. Although the input of water in the subduction cycle through sediments and the crust is fairly well constrained [*Plank and Langmuir*, 1998; *Schmidt and Poli*, 1998], little is known about the degree and extent of serpentinized mantle which may contain as much water as the crust and sediments and significantly influence the water budget at subduction zones [*Billen*, 2009; *Hacker et al.*, 2003; *Rüpke et al.*, 2004; *van Keken et al.*, 2011].

[3] Serpentine is a hydrous magnesium silicate containing up to 13 wt% water and is stable down to depths of ~200 km (~720°C at 2 GPa) [*Ulmer and Trommsdorff*, 1995]. The dehydration of serpentine minerals at depth results in fluid release triggering intermediate-depth earthquakes [*Brudzinski et al.*, 2007; *Peacock*, 2001] and melting in the mantle giving rise to arc magmatism [*Rüpke et al.*, 2002]. In order to serpentinize the mantle, pathways are necessary for the fluid to migrate down to depth. Growing observational evidence suggests that the incoming oceanic lithosphere at subduction zones (e.g., Nicaragua, north and central Chile, Tonga) is tectonically and chemically modified as it bends and further deforms between the flexural outer rise and the axis of the trench [*Grevemeyer et al.*, 2007; *Grevemeyer et al.*, 2005; *Ranero et al.*, 2003]. Seafloor mapping [*Grevemeyer et al.*, 2005; *Ranero et al.*, 2003] and earthquake mechanisms in this area [*Lefeldt and Grevemeyer*, 2008; *Lefeldt et al.*, 2009] are consistent with bending-related normal faulting or 'bend-faulting' occurring in this region. More recently, numerical studies have shown that faults are generated at shallow depths offshore due to plate bending and progressively deepen as the plate approaches the trench-axis [*Faccenda et al.*, 2009]. Additionally, subhydrostatic or inverted pressure gradients develop within the fault planes during plate bending driving downward fluid flow. At a number of subduction zones, heat flow measurements on the incoming oceanic plate indicate a systematic and significant (up to ~90%) decrease in surface heat flow as the plate approaches the trench axis [*Grevemeyer et al.*, 2005]. Since sedimentation is minor in some of these subduction zones (e.g., middle America, northern Chile, Tonga), the only plausible mechanism for this reduced heat flow is downward migration of seawater into the region undergoing bend-faulting. Seawater migration to mantle depths would cause, under appropriate temperature conditions, the hydration reaction between water and peridotite to form serpentine. Indeed, the reflectivity that defines the faults observed in seismic reflection images [*Grevemeyer et al.*, 2005; *Ranero et al.*, 2003] suggests that the physical properties of the initially dry peridotitic rock have been transformed to partially serpentinized peridotite within/around these fault zones.

[4] Velocity reduction in the trench-outer rise prior to subduction is a profound feature of most subduction zones. Seismic compressional wave velocity decreases during serpentinization from nearly ~8.0–8.2 km/s in unaltered peridotites to ~4.5 km/s at 100% transformation of peridotite to serpentinite [*Carlson and Miller*, 2003]. Thus, seismic velocity models derived from tomographic inversions can provide important information on the state of hydration at trenches prior to subduction. Offshore southern central Chile near Chiloe Island, the incoming plate is ~14 Ma. Approaching the Chile trench, uppermost mantle seismic velocities are significantly reduced, suggesting that the structure of both the oceanic crust and uppermost mantle has been altered [*Contreras-Reyes et al.*, 2007]. The decrease in seismic velocity starts at the outer rise, ~120 km from the trench axis, and continues into the trench, reaching values of ~7.8 km/s at the trench axis, which indicates up to ~9% partial serpentinization of the uppermost mantle [*Carlson and Miller*, 2003]. Offshore Nicaragua the subducting plate is 24 Ma where anomalously low P wave speeds of the uppermost mantle rocks of 7.6–7.8 km/s are found, suggesting up to 12–17% partial serpentinization [*Grevemeyer et al.*, 2007; *Ivandic et al.*, 2008]. Later investigations revealed up to 40% serpentinization at the Nicaraguan margin reaching depths of ~12 km beneath the Moho [*van Avendonk et al.*, 2011]. At the Tonga trench, in approximately 90 Ma lithosphere, outer rise bend-faulting caused prominent 10 km wide and 1.5 km deep grabens to form. These are associated with

even lower crustal and mantle velocities. Mantle velocities here are as low as 7.3 km/s, indicating up to 25% partial serpentinization. *Contreras-Reyes et al.* [2011] used gravity data in combination with seismic data to yield the depth interval through which density (and hence seismic velocity) has been changed which showed a 24 km thick portion of hydrated mantle.

[5] In conclusion, seismic velocity reduction at deep-sea trenches is a common feature, and indicates that the seismic and density structure of the incoming plate systematically changes as it approaches the trench. Mantle velocity reduction can be explained by serpentinization and depending on the age of the subducting plate, it suggests that serpentinization may affect several tens of kilometers of the uppermost lithospheric mantle of the subducting lithosphere. However, seismic refraction studies in oceanic crust generally suffer from the fact that the low wave speed gradient in the upper mantle restricts seismic ray penetration to the uppermost 2–3 km of the mantle. Therefore, these experiments have a difficult time capturing the total depth interval in which the seismic wave speed has been changed by serpentinization. Additionally, starting models for seismic inversions commonly assume a gradient of mantle serpentinization with maximum serpentinization at the Moho which decreases with depth [*Contreras-Reyes et al.*, 2007]. Although, it has been shown that this does not affect the final velocity model, it is unclear if a different pattern of serpentinization could yield similar results. Therefore, although geophysical methods are crucial to understand hydration processes at the outer-rise, direct estimates from seismic and gravity surveys can also only provide averages and suffer from limited resolution at depth. To complement the insights gained from seismic experiments, we have developed a reaction-transport model that allows us to better quantify how much and at what depth bending related serpentinization occurs. The model couples a pure-water porous convection model with a kinetics based serpentinization model [*Emmanuel and Berkowitz*, 2006; *Iyer et al.*, 2010].

## 2. Mathematical Model

[6] The hydrological regime of the outer-rise region is closely linked to plate deformation making it challenging to model. So far, *Faccenda et al.* [2009] presented the only model that resolves plate deformation with fluids but neglected reactive flow. In this study we focus on one aspect and that is the role of serpentine reaction kinetics on fluid flow and plate hydration. For this purpose we use a simplified setup, in which plate deformation/movement is kinematically prescribed and fluid flow is driven by buoyancy and a prescribed amount of porosity opening. We thereby study a complementary end-member of the problem addressed by *Faccenda et al.* [2009].

### 2.1. Hydrothermal Convection Model

[7] Hydrothermal convection can be described by three governing equations. Here we follow a treatment similar to previous numerical experiments [*Coumou et al.*, 2006; *Emmanuel and Berkowitz*, 2006; *Iyer et al.*, 2010; *Theissen-Krah et al.*, 2011]. Single (fluid) phase Darcy flow in a deformable matrix can be written as:

$$\vec{q} = \phi(\vec{u}_f - \vec{u}_m) = -\frac{k}{\mu_f}\left(\nabla P - \rho_f \vec{g}\right) \tag{1}$$

where $\vec{q}$ is the Darcy velocity, $\vec{u}_f$ is the pore velocity, $\vec{u}_m$ is the matrix velocity, $\phi$ is the porosity, $k$ is the matrix permeability, $P$ is the fluid pressure and $\mu_f$ and $\rho_f$ are the fluid viscosity and density, respectively (see Table S1 in the auxiliary material for complete list of notations and values).[1] The mass conservation equation can be written as (2) which can be combined with (1) and by splitting density changes into its pressure and temperature parts to derive the fluid pressure equation (3).

$$\frac{\partial \phi \rho_f}{\partial t} = -\nabla \cdot \left(\phi \rho_f \vec{u}_f\right) \tag{2}$$

$$\phi \rho_f \beta_f \frac{\partial P}{\partial t} = \nabla \cdot \left[\frac{k \rho_f}{\mu_f}\left(\nabla P - \rho_f \vec{g}\right)\right] + \phi \rho_f \alpha_f \frac{\partial T}{\partial t} - \rho_f \frac{\partial \phi}{\partial t}. \tag{3}$$

[8] Note the solid terms in (3) are neglected for horizontal solid flow and incompressible matrix [*Theissen-Krah et al.*, 2011]. The third equation describes energy conservation, including advective and conductive heat transport:

$$\left[(1-\phi)\rho_m c_{pm} + \phi \rho_f c_{pf}\right]\frac{\partial T}{\partial t} = -\rho_f c_{pf} \vec{q} \cdot \nabla T - \left[(1-\phi)\rho_m c_{pm} + \phi \rho_f c_{pf}\right]\vec{u}_m \cdot \nabla T + \nabla \cdot (\kappa \nabla T). \tag{4}$$

[1] Auxiliary materials are available in the HTML. doi:10.1029/2012GC004304.

[9] Fluid properties of density, viscosity and specific heat capacity are treated as functions of pressure and temperature and are computed at every time step using PROST (O. Bauer, PROST: Properties of Water and Steam, 1998, http://fluidos.etsii.upm.es/profesores/Jaime_Carpio/Fumatas_negas/PROST%20Properties%20of%20Water%20and%20Steam.htm). PROST is a C library that uses IAPWS IF84 standard formulation to calculate (pure) water and steam properties.

## 2.2. Serpentinization

[10] One of the most important and ubiquitous hydration reactions occurring in the oceanic lithosphere is the serpentinization of ultramafic rocks, which alters both the chemical and physical properties of the lithosphere. The determination of a single rate law describing the progress of serpentinization is complex. Previous studies have shown that the rate of serpentinization is affected by the initial starting material, grain size distribution, temperature, water supply, intergranular diffusion and serpentine dissolution rate [*Malvoisin et al.*, 2012; *Martin and Fyfe*, 1970; *Wegner and Ernst*, 1983]. Of these, temperature and grain size have first-order effects on the rate of serpentinization when water is available for the reaction to proceed [*Malvoisin et al.*, 2012]. Experimental data indicate that the rate of serpentinization can be characterized by a temperature-dependent bell-shaped curve [*Malvoisin et al.*, 2012; *Martin and Fyfe*, 1970; *Wegner and Ernst*, 1983]. The peak reaction temperature determined in these experiments lies between 270°C and 300°C. An important question is if reaction kinetics matter over the time frames typical of subduction zones. For example, the amount of time required for a fault 100 km seaward of the trench to subduct at a velocity of 10 cm/yr is 1 Myr. This duration is similar to the time over which serpentinization takes place in nature which is known to be orders of magnitude larger than is observed in experiments [*Fruh-Green et al.*, 2003; *Malvoisin et al.*, 2012; *Martin and Fyfe*, 1970; *Skelton et al.*, 2005]. Moreover, most faulting occurs close to the trench axis [*Ranero et al.*, 2003] which further decreases the period over which serpentinization will be active. Therefore, it appears likely that the rate of serpentinization in subduction settings is controlled by both, reaction kinetics and water supply. In this parameterization, it reaches a maximum value at ~270°C with essentially no reaction occurring below and above 100 and 400°C, respectively. The incorporation of the rate of serpentinization into the above equations is described by *Emmanuel and Berkowitz* [2006]; we expand on their approach. The rate of alteration per unit volume that *Emmanuel and Berkowitz* [2006] used is,

$$\frac{\partial \rho_{fo}}{\partial t} = -K_r \rho_{fo} \tag{5}$$

where $\rho_{fo}$ is the remaining mass of forsterite per unit volume and,

$$K_r = Ae^{-b(T-c)^2} \tag{6}$$

where $T$ is the absolute temperature. Experimental data as well as the presence of relict olivine in natural samples suggests that water supply is also key for the reaction to reach completion and may affect the reaction rate [*Macdonald and Fyfe*, 1985; *Martin and Fyfe*, 1970]. In addition, the amount of net-porosity opening, which limits the amount of fluid available for reaction that can potentially be supplied via bend-faulting, is also poorly constrained. Therefore, in order to capture the effect of water supply on the rate of serpentinization, we modify (5) to include porosity which we use to parameterize a linear functional dependence on the availability of water,

$$\frac{\partial \rho_{fo}}{\partial t} = -K_r \rho_{fo} \phi \tag{7}$$

The rate of serpentinization thus depends on the remaining fraction of unreacted rock, temperature, porosity, and the rate coefficient $K_r$. Serpentinization of 'dry' rocks results in the consumption of large amounts of water and the generation of heat due to the exothermic nature of the reaction. (2) and (4) are modified in order to account for these effects [*Emmanuel and Berkowitz*, 2006],

$$\frac{\partial \phi \rho}{\partial t} = -\nabla \cdot \left( \phi \rho_f \vec{u}_f \right) + R \tag{8}$$

$$R = w \frac{\partial \rho_{fo}}{\partial t} \tag{9}$$

where $R$ is the volumetric rate of fluid consumption and acts a sink term in the flow equation and $w$ is the water to forsterite mass ratio of the reaction. Exothermic heat generated during serpentinization (~300°C increase in temperature for complete serpentinization) is added as a source term in (4) [*Emmanuel and Berkowitz*, 2006],

$$\left[ \phi \rho_f c_{pf} + (1-\phi) \rho_m c_{pm} \right] \frac{\partial T}{\partial t} = -\rho_f c_{pf} \vec{q} \cdot \nabla T - \left[ \phi \rho_f c_{pf} + (1-\phi) \rho_m c_{pm} \right] \vec{u}_m \cdot \nabla T + \nabla \cdot (\kappa \nabla T) + Q \tag{10}$$

where

$$Q = -H\frac{\partial \rho_{fo}}{\partial t} \tag{11}$$

Q is a source term that accounts for the latent heat effect of the serpentinization reaction and H is defined as the heat of reaction per unit mass of forsterite.

## 2.3. Permeability and Porosity Model

[11] The initial porosity ($\phi_0$) is constant and the permeability is depth dependent:

$$k = k_s \exp(fz) \tag{12}$$

where $k_s$ is the permeability at the seafloor, $f$ is a decay constant and $z$ is the depth in meters. The damage zone generated by the initiation and growth of bend-faulting as the incoming plate progresses toward the trench is simulated by a linear increase in porosity toward a maximum ($\phi_{\max}$) at the trench.

[12] The permeability and porosity of rocks at depth remain difficult to directly determine. Closure of pore space and micro cracks with increasing lithostatic pressure will lead to a reduction in porosity and permeability. On the other hand, bend-faulting of the downgoing slab can increase the porosity and permeability of the lithosphere. Although permeability of rocks in the upper 500 m of the oceanic lithosphere varies between $10^{-10}$ and $10^{-14}$ m$^2$, the measured permeability of rocks at a depth between 500 and 1300 m decreases from $5 \times 10^{-16}$ to $5 \times 10^{-18}$ m$^2$ [*Fisher*, 2005] which is comparable to the value ($5 \times 10^{-17}$ m$^2$) used in the model and other recent studies [*Faccenda et al.*, 2009]. The model used is on the km scale and the top 500 m of crust is ignored as we are focusing on mantle serpentinization processes. Additionally, hydration reactions influence hydraulic properties of the affected rock. Evidence for both closure of existing fractures and generation of new fractures has been observed in nature and experiments during serpentinization [*Andreani et al.*, 2004; *Iyer and Podladchikov*, 2009; *Iyer et al.*, 2008a, 2008b; *Okamoto et al.*, 2011]. The serpentine minerals formed are significantly weaker than the original minerals which can further influence deformation [*Escartín et al.*, 1997a, 1997b, 2001]. However, as a quantitative evolution of permeability and porosity during serpentinization reactions is largely unknown, these feedbacks are not implemented in the current version of the model.

## 2.4. Implementation

[13] The governing equations are solved using a 2D finite element approach in combination with an advection scheme. Partial solutions are computed for every time step in the following sequential order: (1) temperature is advected using both the solid subduction velocity and the Darcy velocities; (2) temperature diffusion is resolved; (3) fluid properties and reaction parameters are updated using the pressure from the previous time step and temperature from the current time step; (4) new fluid pressure and porous flow velocities are computed; (5) the degree of mantle hydration is updated using (7); (6) the time step is concluded by advecting the compositional and porosity fields with the subduction velocity.

[14] The fluid pressure equation is obtained by substituting (1) into (8) and is solved using finite elements. The weak form of this equation is derived by the Galerkin method:

$$\begin{aligned}
&\int_\Omega N'\phi\rho_f\beta_f N\tilde{P}^n d\Omega + \int_\Omega \frac{\partial N'}{\partial x}\frac{k\rho_f}{\mu_f}\Delta t\frac{\partial N\tilde{P}^n}{\partial x}d\Omega \\
&+ \int_\Omega \frac{\partial N'}{\partial y}\frac{k\rho_f}{\mu_f}\Delta t\frac{\partial N\tilde{P}^n}{\partial y}d\Omega = \int_\Omega N'\phi\beta_f\rho_f N\tilde{P}^o d\Omega \\
&+ \int_\Omega N'\Delta t\phi\alpha_f\rho_f N\left(\frac{\partial T}{\partial t}\right)d\Omega - \int_\Omega N'\rho_f N\left(\frac{\partial \phi}{\partial t}\right)d\Omega \\
&+ \int_\Omega N'\Delta t N R d\Omega - \int_\Omega \frac{\partial N'}{\partial y}\frac{k}{\mu_f}\Delta t\vec{g}N\tilde{\rho}_f^2 d\Omega \\
&+ \oint_\Gamma N'\frac{k\rho_f}{\mu_f}\Delta t\frac{\partial N\tilde{P}}{\partial x}d\Gamma + \oint_\Gamma N'\frac{k\rho_f}{\mu_f}\Delta t\frac{\partial N\tilde{P}}{\partial y}d\Gamma \\
&+ \oint_\Gamma N'\frac{k}{\mu_f}\Delta t\vec{g}N\tilde{\rho}_f^2 d\Gamma
\end{aligned} \tag{13}$$

where pressure is expressed as $P = N\tilde{P}$, $N$ are quadratic shape functions for 6 six node triangle elements and $\tilde{P}$ are the nodal pressures. Rock properties are assumed constant over an element. Note how the partial integration is performed also on the right-hand side of the equation thereby providing a line integral over the (boundary) Darcy velocities. The pressure solution is obtained by implementing (13) into a modified version of the Matlab-based FEM solver MILAMIN [*Dabrowski et al.*, 2008].

[15] Derivatives of the pressure solution are used to calculate the updated Darcy velocities that are used in the advection part of the energy equation (4). The velocities are mapped on to the nodes using shape functions and are averaged depending on the number

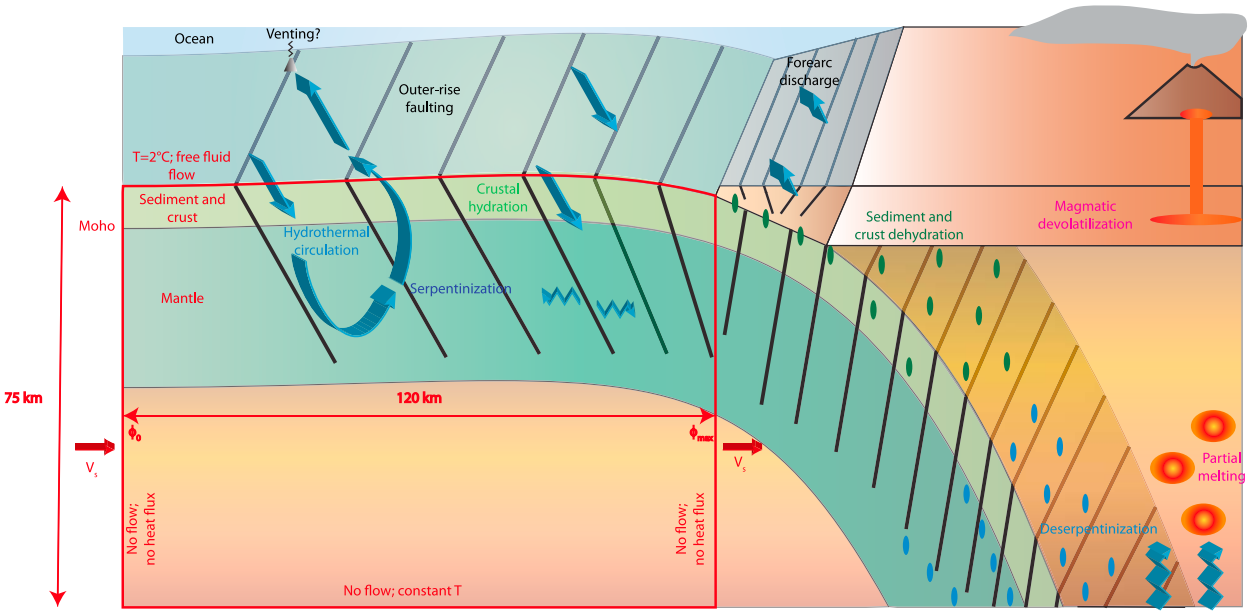


**Figure 1.** Schematic drawing of subduction zone processes. Crustal and mantle hydration, in addition to hydrothermal circulation, occurs at the onset of bending related faulting at the trench outer-rise. Water trapped with pore space and hydrous minerals is subsequently released at varying depths resulting in the formation of cold-seeps in the forearc region at shallow depths [*Hensen et al.*, 2004] and arc melting due to deep fluid release during crustal dehydration and deserpentinization [*Ishikawa and Nakamura*, 1994]. Incomplete dehydration of the mantle may result in the recycling of water into the mantle [*Rüpke et al.*, 2004]. Red box and text denotes model setup. See text for details.

of elements sharing any given node. The advection solver uses a semi-Lagrange method based on following characteristics backward through the time step. The diffusion part of equation (4) is again solved with a FEM scheme. This approach is described in more detail in *Iyer et al.* [2010].

## 3. Model Setup

[16] The domains used in the simulations describe an across-trench profile based on the seismic profile from south central Chile [*Contreras-Reyes et al.*, 2007] extending 120 km seaward from the trench and to a depth of 75 km from the seafloor (Figure 1). The mesh consists of six-node triangular elements with approximately 155,000 elements in the simulated domain. Seafloor elevation of the domain is obtained from reflection seismics. Pressure at the top surface reflects the local seafloor depth with the shallowest seafloor lying at a depth of 3.5 km below the sea surface. Temperature is initialized using the error function for the half-space cooling model for old, oceanic lithosphere that is given by [*Turcotte and Schubert*, 2002],

$$T = T_1 - T_0\left[erf\left(\frac{|y|}{2\sqrt{KA}}\right)\right] + T_0 \qquad (14)$$

where $T_1 - T_0 = 1298°C$, $y$ is the corresponding depth ($m$), K is the thermal diffusivity of the rock ($10^{-6}$ m$^2$ s$^{-1}$), $T_0$ is the surface temperature (2°C) and $A$ is the age of the lithosphere (s). The sides of the box used in the simulations are impermeable and insulating. The bottom boundary is impermeable and kept at a constant temperature derived from the half-space cooling model (14). Free flow conditions are imposed at the domain surface where downgoing fluids have a temperature of 2°C. There is no fluid flow or heat flux allowed through the side boundaries. Serpentinization occurs only in the mantle region below the Moho while the crustal region is unreactive in this model. The Moho occurs at a depth of 5.3 and 6.0 km below the slab surface for all simulations based on the south Chilean and Nicaraguan subduction zones, respectively. Pristine lithosphere enters with the plate velocity from the left side of the box while reacted lithosphere is removed from the right side at this rate. Brittle deformation in the incoming slab is connected to the formation of bending-related faulting which in turn would directly depend on the plate curvature as the trench axis is approached. The damage zone generated by these faults is linked to an increase in porosity in the subducting slab. Porosity is initialized to the starting value that increases linearly with time to a maximum value at the trench. Initial

permeability in the simulations decreases exponentially with depth where the surface permeability is $5 \times 10^{-17}$ m$^2$ (12) and initial porosity is constant ($10^{-5}$) throughout the slab. Additionally, permeability and porosity where the temperatures exceeds 600°C (brittle-ductile transition) is limited to $10^{-21}$ m$^2$ and $10^{-5}$, respectively. The depth-extent of faulting and fluid flow (brittle-ductile transition) will, therefore, increase with increasing plate age as colder, old subducting plates are more rigid that younger, hot subducting plates [*Contreras-Reyes and Osses*, 2010; *Goetze and Evans*, 1979; *McNutt and Menard*, 1982]. Another factor that controls the depth of hydration and fluid flow is the neutral plane of deformation during plate bending, which separates the upper part of the incoming plate that undergoes tensional deformation from the lower part that experiences compression. The neutral plane of deformation may therefore be an additional limit to downward fluid flow and thereby hydration reactions [*Contreras-Reyes and Osses*, 2010; *Lefeldt et al.*, 2012; *Seno and Yamanaka*, 1996]. Previous studies have shown that the neutral plane can be related to the thermal structure of the subducting slab and occurs between 300°C and 450°C [*Seno and Yamanaka*, 1996]. Although the depth of these isotherms are lower than the 600°C isotherm, our model is consistent (and complementary) as the reaction kinetics of serpentinization limits the depth of hydration to the 400°C isotherm which is close to the likely location of the neutral plane where tensional stresses tend toward zero and thereby also confines hydration to shallower depths.

## 4. Results and Discussion

[17] The model setup described above is used in two sets of experiments calibrated against geophysical observations of serpentinization at the trench outer-rise to determine the rate of serpentinization in nature and porosity opening associated with bend-faulting. The values of these parameters are subsequently used to resolve the extent of serpentinization that may potentially take place at various global subduction zones.

### 4.1. Calibration Simulations

[18] Plate bending induced faulting and serpentinization was first discovered at the Nicaraguan subduction zone [*Ranero et al.*, 2003], later also addressed by numerical modeling [*Faccenda et al.*, 2009], and has now been observed at multiple convergent margins including Chile. South central Chile is characterized by a relatively thick sediment blanket which may inhibit downward fluid flow [*Contreras-Reyes et al.*, 2007]. On the other hand, the Nicaraguan subduction zone is poorly sedimented which is likely to allow seawater to more easily flow vertically. Additionally, the reactivation of pre-existing faults and the formation of new bend-faults is enhanced offshore Nicaragua, most likely because the tectonic fabric of the incoming plate is nearly parallel to the axis of bending [*Ranero et al.*, 2003] which is not the case for the south central Chilean subduction zone [*Contreras-Reyes et al.*, 2007; *Grevemeyer et al.*, 2005]. Therefore, the south central Chilean and Nicaraguan subduction zones are taken as calibration cases where seawater penetration and hydration of the mantle due to bending-related faulting are low to moderate and high, respectively. The rate of serpentinization is varied linearly from $10^{-12}$ s$^{-1}$ to $10^{-10}$ s$^{-1}$ and the maximum porosity value at the trench is independently varied linearly from $10^{-4}$ to $10^{-2}$. The results for selected values of the above mentioned variables are shown in Figure 2. The ages of the subducting lithosphere for the Chilean and Nicaraguan simulations are 14 and 24 Ma, respectively, and subduct at a velocity of 6.6 and 9.1 cmyr$^{-1}$, respectively [*Angermann et al.*, 1999; *Contreras-Reyes et al.*, 2007; *Ivandic et al.*, 2008]. Porosity opening occurs at a constant rate such that the maximum porosity value is reached at the trench. Serpentinization takes place as fluids flow downward toward the mantle and occurs between 100°C and 400°C with the maximum amount around the 270°C isotherm as predicted by the kinetics of the reaction. The amount of serpentinization gradually increases toward the trench as porosity evolves to higher values due to an increase in bend-faulting. The average amount of serpentinization and the corresponding chemically bound water content in the mantle column at the trench is calculated for each simulation. The amount of serpentinization will, of course, increase with increasing reaction rate and water content. The rate of serpentinization and the porosity opening matching the geophysical observations for the Chilean subduction zone (~9% average serpentinization in the upper 2 km of the mantle), are $8.5 \times 10^{-12}$ s$^{-1}$ and $8.5 \times 10^{-4}$ respectively, which are interpolated from the results obtained in this suite of experiments. This results in a ~10 km thick partially serpentinized mantle with $\sim 2 \times 10^5$ kgm$^{-2}$ water trapped in the mantle column. The maximum water content in the mantle column due to serpentinization at Nicaragua has been estimated at $1.1 \times 10^6$ kgm$^{-2}$ from seismic observations [*van Avendonk et al.*, 2011] which can be obtained from our model if the porosity increases to a maximum value of

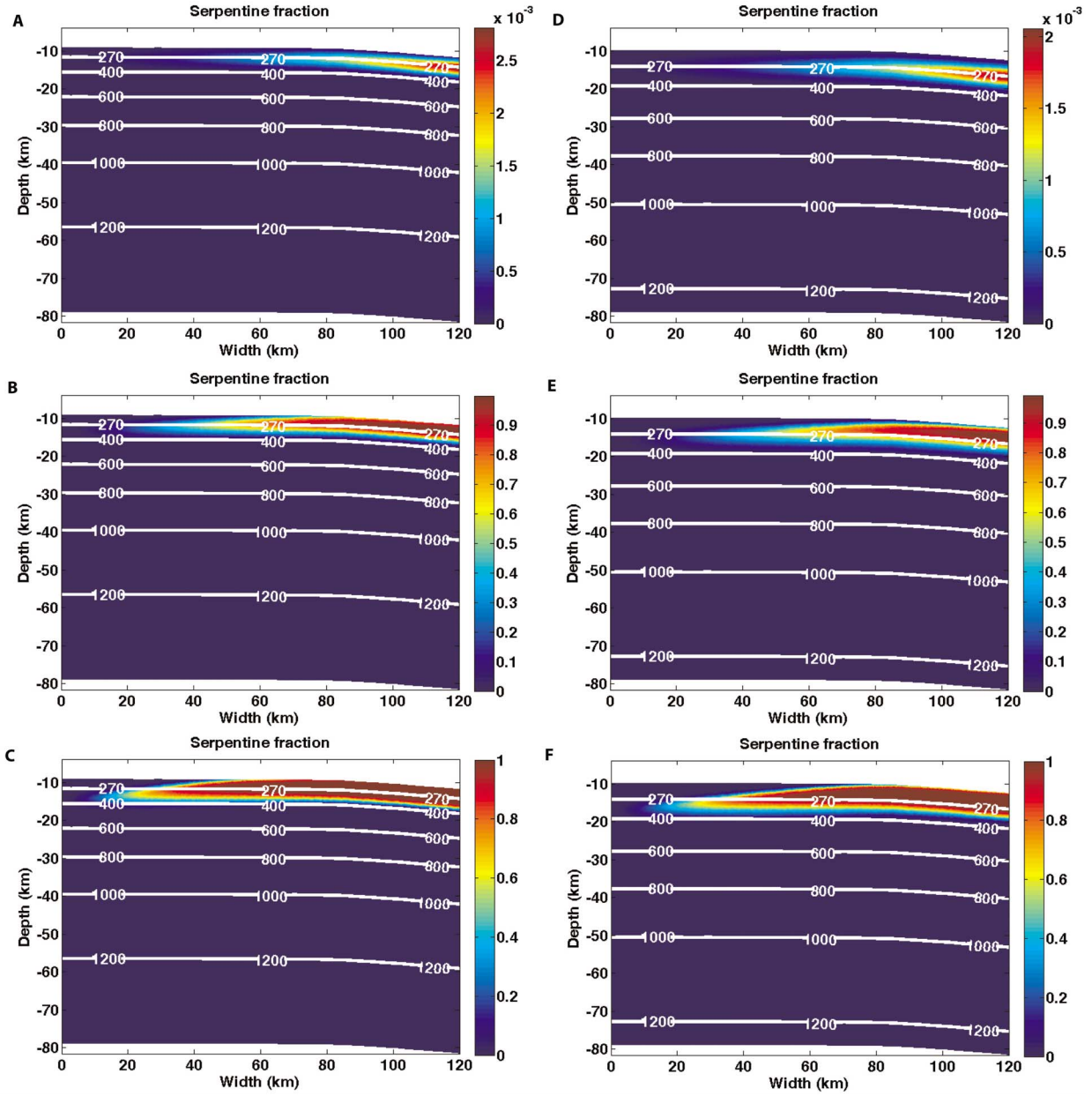


**Figure 2.** Initial temperature and final serpentinization fraction plots for the simulations calibrated against the (a–c) south central Chilean and (d–f) Nicaraguan subduction zones for varying serpentinization rates and maximum porosity opening values. Figures 2a–2c plot the results for the south central Chilean subduction zone for serpentinization rates of $10^{-12}$ $s^{-1}$, $4.34 \times 10^{-11}$ $s^{-1}$ and $10^{-10}$ $s^{-1}$, respectively with corresponding maximum porosity opening values of $10^{-4}$, $5.1 \times 10^{-3}$ and $10^{-2}$. Figures 2d–2f are the results for the Nicaraguan subduction zone with the same parameters. Maximum serpentinization occurs along the initial 270°C isotherm as per the reaction kinetics (Figures 2a and 2d). However, large amounts of serpentinization result in localized heating and shifts the initial 270°C isotherm upwards and displacing the depth of maximum serpentinization (Figures 2b, 2c, 2e, and 2f).

$6 \times 10^{-3}$ at the trench as the increase in fault density is translated to an increase in porosity opening. The rate of serpentinization is chosen to be the same, namely a value of $8.5 \times 10^{-12}$ $s^{-1}$. The results of these simulations are shown in Figure 3. As mentioned in section 2.2, although the combined reaction rates (taking into account the absolute reaction rate, $A$, and porosity (7)) obtained from the calibration simulations are orders of magnitude slower than the rates obtained from experimental results [*Malvoisin et al.*, 2012; *Martin and Fyfe*, 1970], the time required for serpentinization to reach completion

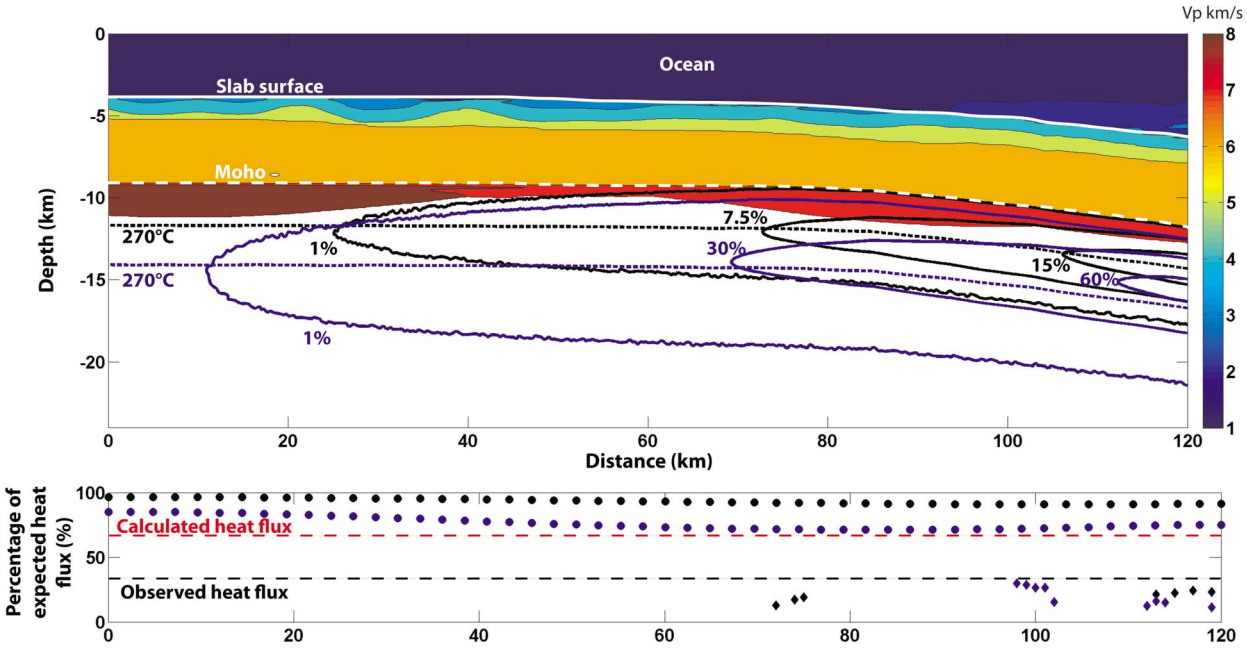


**Figure 3.** (top) Seismic velocity structure from the south central Chilean subduction for a cross-section 120 km seawards of the trench [*Contreras-Reyes et al.*, 2007] (trench at right side). A decrease in seismic velocity to 7.8 km/s is observed in at least the upper 2 km of the mantle corresponding to 9% partial serpentinization. A band of serpentinization is formed due to reaction kinetics (black contours showing percent of serpentinization) with the maximum occurring at the initial 270°C isotherm (black dashed contour). The band of partial serpentinization for the Nicaraguan subduction zone is shown here with blue contours. In this case, the depth of maximum serpentinization is shifted slightly upwards from the initial 270°C isotherm (blue dashed contour) due to the larger amount of heat released by the exothermic serpentinization reaction. (bottom) Difference between calculated heat flux at the surface for both simulations (circles; black - Chilean simulation and blue - Nicaraguan simulation) and the observed heat flux at these subduction zones [*Grevemeyer et al.*, 2005] (diamonds with the same color scheme) normalized as a percentage of the expected conductive heat flux for the plate ages is at least 40%. Note: The heat flow data shown for the Chilean subduction zone was measured at a different bend-fault site in northern Chile, while the Nicaraguan heat flow data is co-located with the seismic measurements.

in the simulations is similar to the duration of serpentinization observed in natural systems ($10^4$–$10^6$ years) [*Fruh-Green et al.*, 2003; *Skelton et al.*, 2005]. The reaction rate used in this study, therefore, reflects more closely the rate of reaction occurring in nature and is used to match observations obtained by geophysical methods.

## 4.2. Global Subduction Zone Simulations

[19] After having calibrated the model at the south Chile and Nicaraguan margins, we now use this model to study the possible global variation of bend-fault serpentinization. The setup used to conduct global simulations is the same as that used in the calibration experiments. We use values for maximum porosity opening and serpentinization rates obtained from the Chilean simulation to study serpentinization at subduction zones with moderate faulting, while the maximum porosity opening value obtained from the Nicaraguan simulation is our upper limit to the reaction in regions where pervasive bend-faulting is anticipated. In these experiments, the age of the subducting lithosphere and the subduction velocity are independently varied from 5 to 185 Ma and 2 to 20 cmyr$^{-1}$, respectively. Selected results from both simulation sets are shown in Figures 4 and 5. The amount of serpentinization and the corresponding water trapped in the partially hydrated mantle depends on both variables. On the one hand, the temperature gradient is lower in older oceanic lithosphere, thereby increasing the depth interval where serpentinization temperatures are favorable. On the other hand, the amount of serpentinization in the mantle is restricted by the residence time of bend-faults before subduction that inversely depends on the speed of subduction since the width of the bend-fault region has only a weak dependence on the age of the subducting plate (Figures 6a and 6c). Very

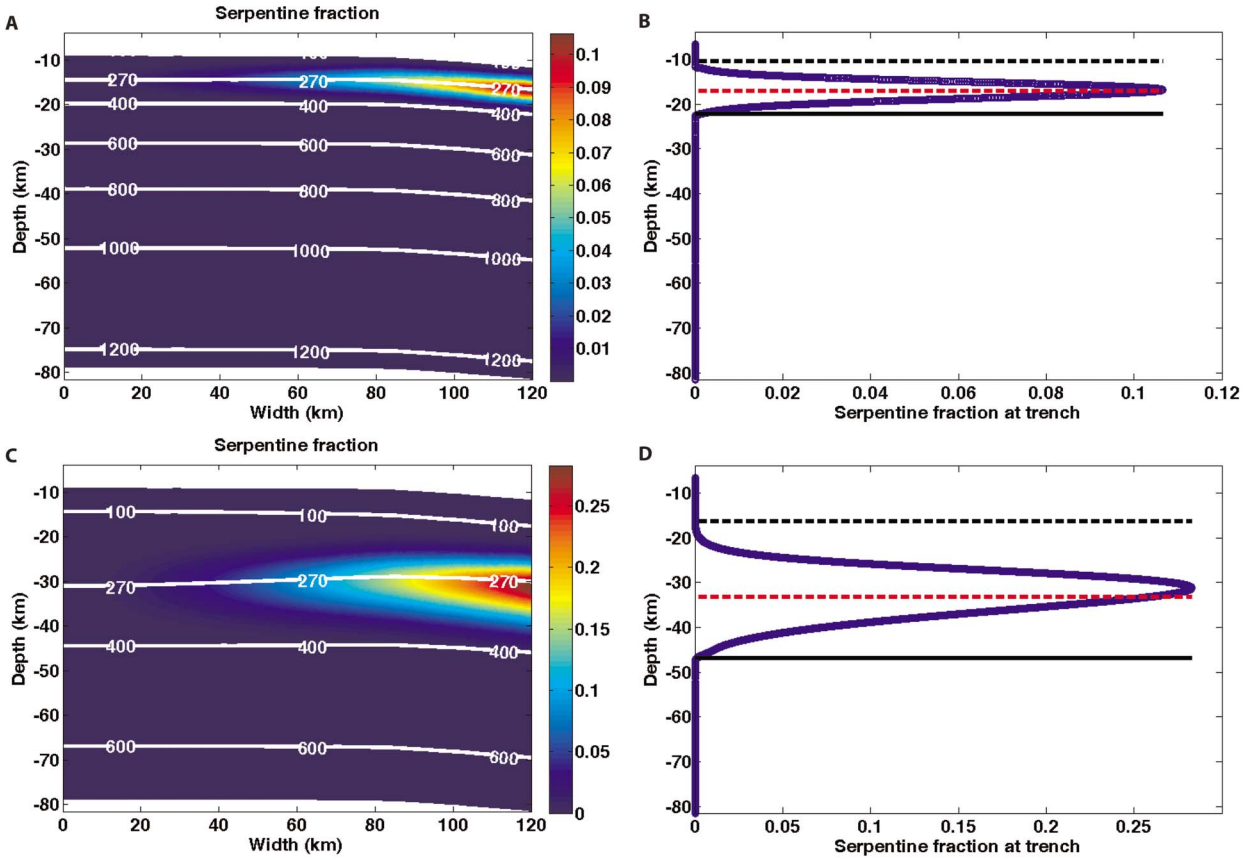


**Figure 4.** Plots of the final thermal structure (white contours), serpentine fraction and the depth of maximum serpentinization for subduction zones with ages and subduction velocities of (a and b) 25 Ma and 12 cm/yr and (c and d) 185 Ma and 4 cm/yr using the parameters obtained from the Chilean simulation results. The end results shown here for the fast and slow subduction zones are obtained after a period of 1 and 3 Myr, respectively. The dashed black, dashed red and solid black lines in Figures 4b and 4d are the initial 100°C, 270°C and 400°C isotherms, respectively. The relatively high degree of serpentinization occurring in the second simulation, in conjunction with the exothermic nature of the reaction, results in an slight upward shift of the temperature isotherms (Figure 4c). The depth at which maximum serpentinization occurs is, therefore, also shifted (Figure 4d).

young (hot) subduction zones with fast subduction rates and low to moderate bend-faulting have low water contents with a minimum of $1.6 \times 10^4$ kgm$^{-2}$ water in the lithosphere mantle column at the trench axis, while old (cold) subduction zones with slow subduction rates and intense bending-related faulting are predicted to be more highly serpentinized with a maximum calculated bound-water content at the trench axis of $5.1 \times 10^6$ kgm$^{-2}$. Although the pattern of serpentinization observed here is very different from previous studies, the water content in partially serpentinized mantle is comparable [*Rüpke et al.*, 2004; *Schmidt and Poli*, 1998]. It should, however, be noted that these numbers probably describe the upper limit of mantle serpentinization as the geophysical observations with which they are calibrated assume that the reduction in seismic velocity is wholly due to mantle serpentinization at the trench outer-rise and ignore the contribution of fracturing. Eventually our results should be further explored in dynamic models that account for matrix deformation in order to quantify how serpentinization reactions affect the strength of bending plates. *Conrad and Hager* [1999] pointed to the high fraction of a slab's potential energy that is necessary to bend it. It might well be that serpentinization through rheological weakening (and expansion in solid volume) can promote plate bending without 'over-reducing' the slab's density, so that subduction remains self-preserving. Evidence of lithospheric weakening at the trench outer-rise has been observed at various subduction zones and has been attributed to intense deformation and an increase of fluid pressure [*Billen and Gurnis*, 2005; *Contreras-Reyes and Osses*, 2010]. However, an increase in the amount of serpentinization with increasing plate age may also play

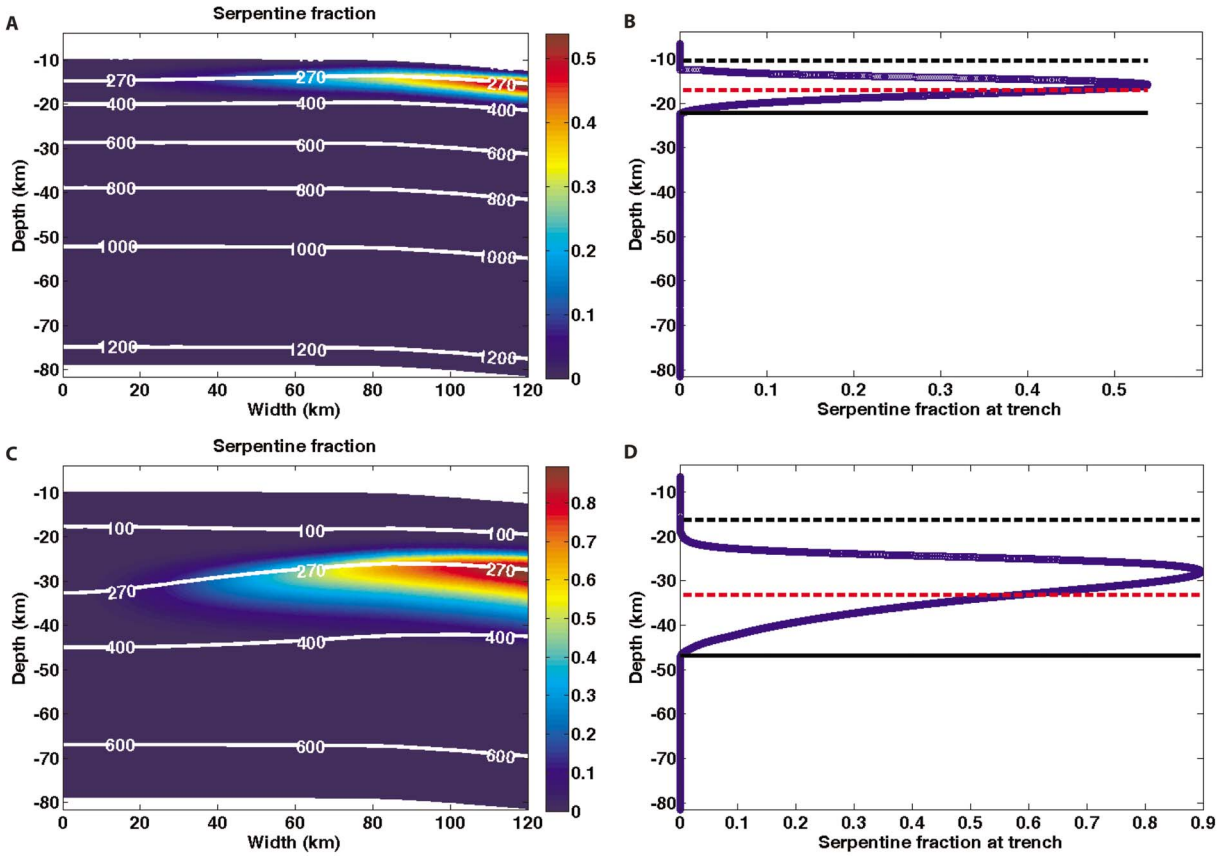


**Figure 5.** Plots of the final thermal structure (white contours), serpentine fraction and the depth of maximum serpentinization for subduction zones with ages and subduction velocities of (a and b) 25 Ma and 12 cm/yr and (c and d) 185 Ma and 4 cm/yr using the parameters obtained from the Nicaraguan simulation results. The end results shown here for the fast and slow subduction zones are obtained after a period of 1 and 3 Myr, respectively. The dashed black, dashed red and solid black lines in Figures 5b and 5d are the initial 100°C, 270°C and 400°C isotherms, respectively. The relatively high degree of serpentinization occurring in the second simulation, in conjunction with the exothermic nature of the reaction, results in an significant upward shift of the temperature isotherms (Figure 5c). The depth at which maximum serpentinization occurs is, therefore, also shifted (Figure 5d).

a role in reducing the effective strength of the downgoing slab due to the presence of hydrous minerals [*Escartín et al.*, 2001].

## 4.3. Serpentinization and Heat Flux

[20] Serpentinization also results in an overall decrease in surface heat flux measured at the trench-axis (Figures 6b and 6d). The reaction forces a downward fluid motion from the slab surface due to the reaction's net consumption of seawater. However, an increase in the amount of serpentinization does not directly correlate with a decrease in the heat flux measured at the seafloor; the reduction in heat flux is lower in the slowest subduction zones than at relatively faster ones even when the extent of serpentinization is larger (Figures 6b and 6d). This is due to exothermic heat generation by the reaction that for slow moving plates has enough time to diffuse toward the surface. The competition between downward fluid migration, heat generation and the time available for thermal diffusion is the reason why the reduction in heat flux at very slow subduction zones is smaller even if more serpentinization occurs.

[21] Very low measured seafloor heat flux values that systematically decrease toward the trench axis are also observed at subduction zones with bend-faults [*Grevemeyer et al.*, 2005]. The heat fluxes at the trench measured at the Nicaraguan and central Chilean subduction zone are as low as 10% and 14%, respectively, of the expected conductive values [*Grevemeyer et al.*, 2005]. Surface heat fluxes calculated for 'one-pass' or minimum water flow

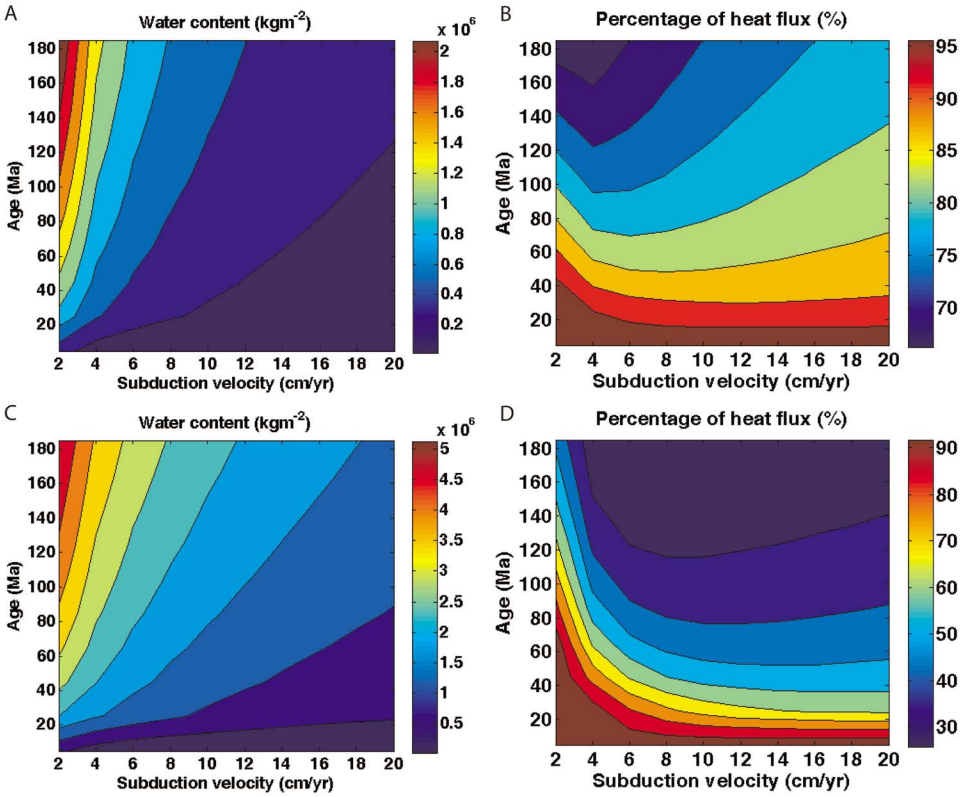


**Figure 6.** (a and c) Predicted amount of water present in serpentine minerals in the mantle column at the trench and (b and d) the percentage of heat flux relative to the conductive values due to hydration prior to subduction based on the parameters obtained from the Chilean and Nicaraguan subduction zones, respectively. The results are from simulations where the age of the incoming lithosphere and the subduction velocity have been independently and systematically modified to span the global range.

experiments (Figure 7a) to serpentinize at the Chilean and Nicaraguan subduction zones are 3–5 times higher than observed values suggesting locally more vigorous hydrothermal convection possible along high-permeability bend-faults. If a component of active hydrothermal flow is also present, then sea-floor heat fluxes can be significantly reduced in the downwelling limbs of active hydrothermal cells, and we believe these cells will naturally align with the bend-faults themselves. Previous work has also shown that strong hydrothermal circulation restricted to the uppermost crust may explain the heat flux anomalies observed at convergent margins [*Kummer and Spinelli*, 2009; *Spinelli and Wang*, 2008, 2009]. We can explore some aspects of active hydrothermal circulation in these 2D models. For example, the experiment in Figures 7b, 8a, and 8c is a Chilean subduction zone-like simulation where the rate of serpentinization and the porosity opening used in this experiment are the same as those used in the 'best fitting' one-pass calibration experiment. The only difference here is that the surface permeability is increased by an order of magnitude ($5 \times 10^{-16}$ m$^2$) while maintaining its depth dependency. In this case, vigorous hydrothermal convection occurs, resulting in numerous active convection cells that perturb the initial thermal structure (Figure 7b). Because of this, serpentinization is less regular and does not form the banded pattern observed in the one-pass experimental conditions (Figure 8a). However, in spite of the uneven pattern of serpentinization, the highest degree of serpentinization averaged over a complete convection cell between 105 and 120 km still forms around the depth of the initial 270°C isotherm (Figure 8c). Moreover, the average water content calculated for the partially serpentinized mantle within this region ($3.0 \times 10^5$ kgm$^{-2}$) differs only 20% from the chemically bound water content ($2.4 \times 10^5$ kgm$^{-2}$) determined from the calibration experiment with the lower surface permeability. However, this mode of vigorous across-trench, hydrothermal circulation is rather improbable due to the high lithospheric permeabilities required and is probably confined to within the damaged fault plane

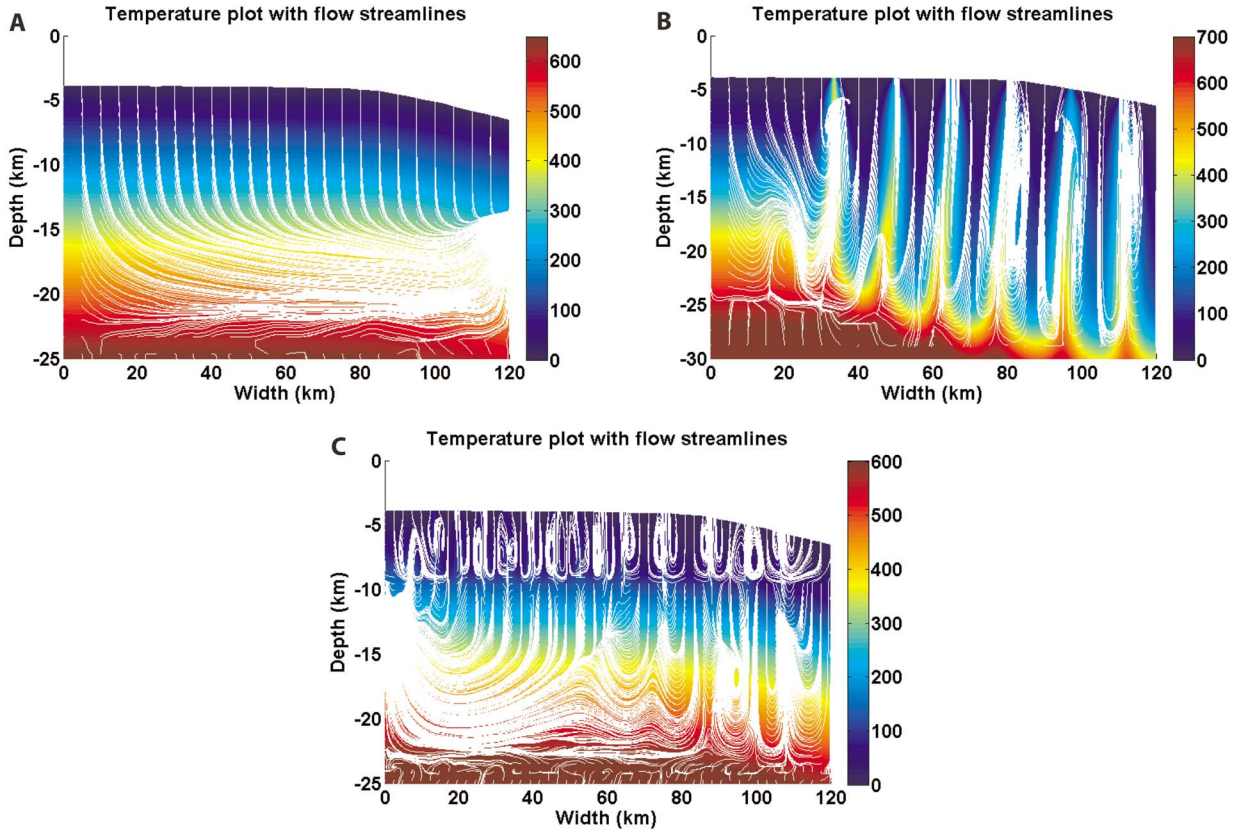


**Figure 7.** (a) The thermal structure and downward fluid flow resulting from mantle serpentinization at the south central Chilean subduction from the calibration simulation after 1.82 Myrs. (b and c) Similar plots from experiments where the surface permeability is increased ($k_s = 5 \times 10^{-16}$ m$^2$) and where the crustal permeability is constant ($k_{crust} = 5 \times 10^{-15}$ m$^2$), respectively. The increased permeability in the latter two simulations generates vigorous hydrothermal convection and modifies the thermal structure of the incoming plate.

itself (along-trench profile). Furthermore, mantle serpentinization patterns and amounts obtained from the 'one-pass' flow simulations should remain relatively unchanged if vigorous convection occurs only in the upper crustal region. An experiment with a relatively high crustal permeability ($5 \times 10^{-15}$ m$^2$) and mantle permeabilities similar to the previous experiment results in the formation of convection cells largely restricted to the subducting crust (Figure 7c). Comparable to the 'one-pass' experiments, a band of serpentinized mantle is formed which undulates slightly (Figure 8b) due to presence of overlying convection cells with the maximum amount of serpentinization occurring very close to the initial 270°C isotherm (Figure 8c). In spite of its similar patterns and amounts of partial serpentinization, the experiments with active hydrothermal convection show a drastic decrease in the measured surface heat flux in the downflow zones of the convection cells when compared to the simulation with one-pass downward fluid flow (Figure 8d). This reduction in seafloor heat flux is similar to the reduction seen in Figure 3, which implies that active hydrothermal flow indeed occurs in this region of subduction bend-faulting. It is also likely that vigorous convection is confined to the crustal region of the bend-fault in the along-trench direction where permeability is expected to be higher. However, a 3D convection model is needed to properly assess this mechanism in detail. Preliminary exploration using our 2D model with higher permeabilities shows that the surface heat flux can be significantly lowered if convection occurs without changing the net amount of serpentinization. We prefer here to report on the minimum water-uptake experiments, as they clearly demonstrate, by their inability to match the observed reduction in surface temperature gradients, that additional 'active' hydrothermal circulation occurs during bend-faulting. Predicted values of the bound-water content and heat flux reduction due to minimum water uptake serpentinization of the mantle for

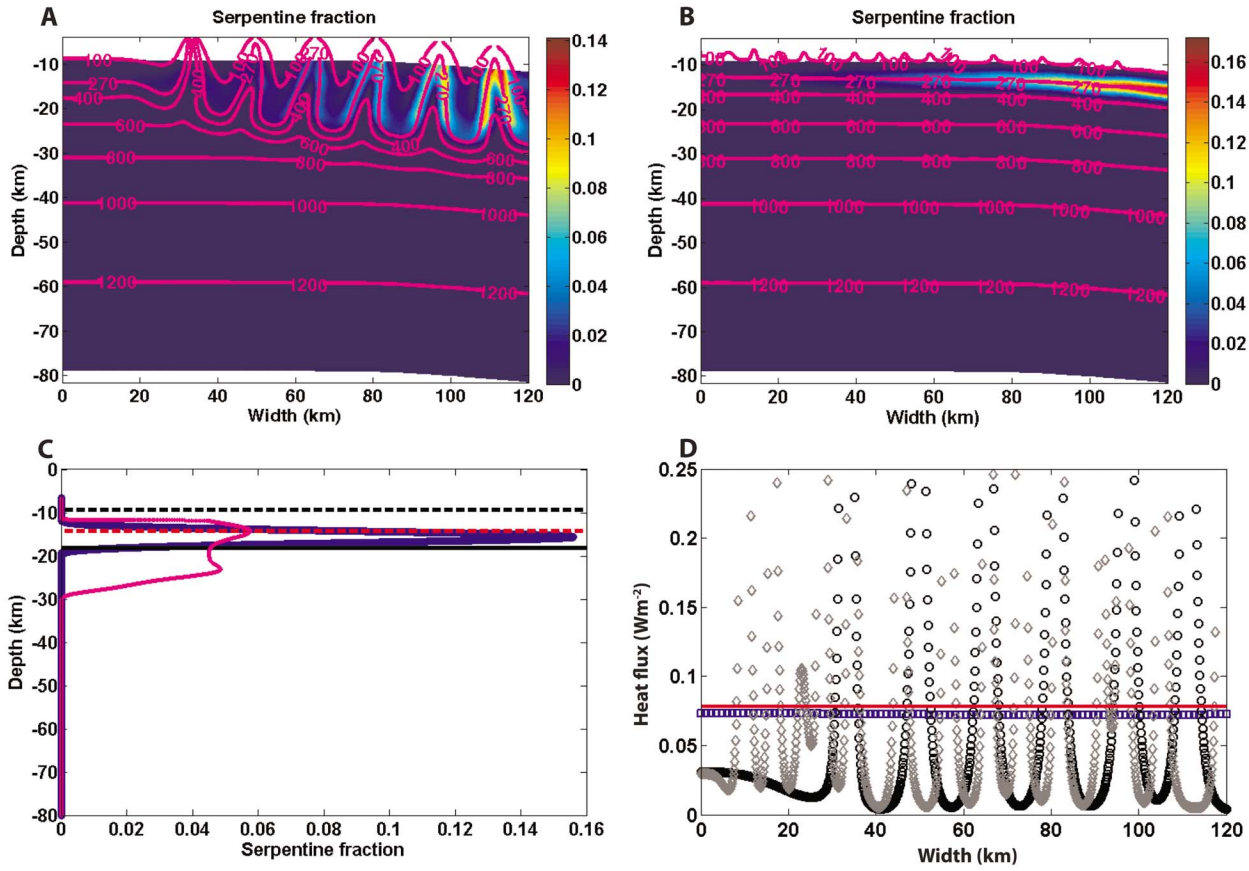


**Figure 8.** (a and b) The thermal structure and the amount of serpentinization after 1.82 Myrs for the south central Chilean subduction zone with a plate age of 14 Ma and a subduction velocity of 6.6 cm/yr. All parameters are the same as those obtained from the Chilean benchmark simulations except a relatively higher permeability structure ($k_s = 5 \times 10^{-16}$ m$^2$) and crustal permeability ($k_{crust} = 5 \times 10^{-15}$ m$^2$) is used in Figures 8a and 8b, respectively, resulting in hydrothermal convection. (c) The extent of serpentinization versus depth averaged over a single convection cell when the entire lithospheric permeability is increased (105 to 120 km) (magenta dots). The blue squares plot the extent of serpentinization versus depth for the simulation where only the crustal permeability is increased. The dashed black, dashed red and solid black lines are the initial 100°C, 270°C and 400°C isotherms, respectively. The maximum amount of serpentinization in both simulations still occurs at the initial 270°C isotherm. (d) The calculated heat flux at the surface (black circles) in the recharge zones of the convection cells when the entire lithospheric permeability is increased can reach a minimum of ~5% of the conductive value for the same plate age (red line). The heat flux values for the simulation with a constant crustal permeability of $5 \times 10^{-15}$ m$^2$ (gray diamonds) show a similar reduction to the simulation where the permeability of entire lithosphere is increased. The calculated heat flux values (blue squares) of the simulation with the same parameters as those obtained from the benchmark simulation, including permeability, is much closer to the expected conductive value (red line).

a number of subduction zones are given in Table S2 in the auxiliary material.

## 4.4. Serpentinization and Double Benioff Zones

[22] A striking feature of all experiments, including experiments with additional active hydrothermal flow (cf. Figure 7) is the occurrence of a pronounced band of highly serpentinized mantle centered on the incoming 270°C isotherm (Figure 3). This effect is due to temperature dependent kinetic effects of serpentine reaction rates. This mechanism can explain a notable feature in the spacing of the double Benioff zones (DBZs) now observed in several subducting slabs [*Brudzinski et al.*, 2007]. The upper seismic plane of a DBZ is believed to be due to dehydration embrittlement/eclogitization reactions in the crustal section of the subducting slab [*Kerrick and Connolly*, 2001]. Various mechanisms have been previously proposed to explain the generation of the unanticipated lower seismic plane in DBZs such as the unbending of the slab [*Engdahl*

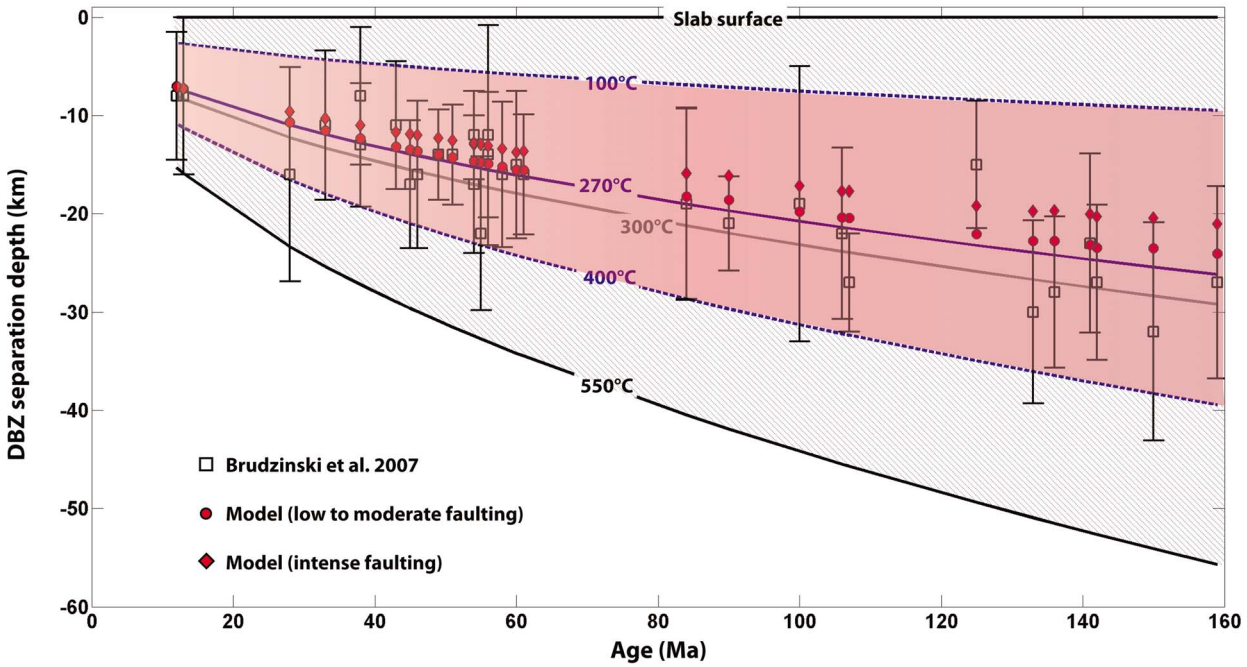


**Figure 9.** The slab-normal distance separating the upper and lower planes of double Benioff zones as a function of the age of the subducting lithosphere. The region where serpentinization would take place at the trench outer-rise in this kinetics-limited partial serpentinization model is shown by the pink region, which correlates closely to the 100°C and 400°C isotherms in the lithosphere at the trench axis. Equilibria serpentinization models would predict a much larger depth interval of serpentinization shown by the gray shaded region, as serpentine is the stable mineral assemblage up to ~550°C. In addition, the depth at which maximum partial serpentinization occurs corresponds to the ~270°C (or 300°C [*Malvoisin et al.*, 2012]) isotherm (the potential depth at which most water is mineral bound) which coincides with the mean observed separation depth between the two Benioff planes [*Brudzinski et al.*, 2007]. Model results deviate slightly upwards from the paleo-270°C isotherm due to the exothermic nature of the serpentinization reaction as these results assume the minimum amount (one-pass) of downward water flow into the serpentinizing lithosphere. Models with greater amounts of (partly non-reactive) hydrothermal flow would lead to predictions for slightly deeper maximum serpentinization still centered around the paleo-270°C isotherm.

*and Scholz*, 1977], thermoelastic stresses [*House and Jacob*, 1982] and plate sagging [*Sleep*, 1979]. However, the presence of DBZs at a variety of subduction zones suggests that two seismogenic layers at intermediate depths can be produced irrespective of the slab's thermal state and stress orientation [*Brudzinski et al.*, 2007]. One of the more favored hypotheses is dehydration of the hydration minerals antigorite and chlorite which increases pore pressure due to fluid release thereby reducing the effective normal stress and promotes brittle failure [*Dobson et al.*, 2002; *Hacker et al.*, 2003; *Meade and Jeanloz*, 1991; *Peacock*, 2001; *Raleigh and Paterson*, 1965] as the cause for the lower region of seismicity. If serpentine breakdown is responsible for DBZ formation, and the depth of the 270°C isotherm, where reaction rates are maximum, controls the distribution of bend-fault serpentinization in the subducting slab, then it should also control the spacing of DBZs. Lithosphere cooling models such as the half-space cooling model [*Turcotte and Oxburgh*, 1967], or the 'plate' cooling model with and without modified parameters [*Parsons and Sclater*, 1977; *Stein and Stein*, 1992] show that the depth of the 270°C isotherm increases with increasing plate age. Strikingly, the predicted depth of the 270°C isotherm as a function of plate age coincides with the dominant separation distance of globally observed double seismic zones [*Brudzinski et al.*, 2007] (Figure 9). The depth at which maximum serpentinization occurs prior to subduction can show upward deviations from the initial 270°C isotherm and is dependent on the amount of serpentinization that has occurred (Figures 4 and 5). Some of the mismatch between the predicted depth of maximum serpentinization and the separation depth of DBZs may be due to the thermal structure of the slab at intermediate depths which may be too cold to induce dehydration in the mantle region that is the most serpentinized [*Rüpke et al.*, 2004; *van Keken et al.*, 2011], or to heterogeneities in bend-fault serpentinization linked to preferential

serpentinization along the deeper extensions of the bend-faults themselves. Recent numerical experiments have shown that fluid release during deserpentinization could lead to updip migration of the released fluid within the colder core regions of the slab along a plane of neutral pressure gradient [*Faccenda et al.*, 2012]. The presence of free fluids and the formation of hydrous minerals lead to the development of a 'double hydrated zone (DHZ)' and may be responsible for intermediate depth seismicity. These findings complement the results shown in this study and may together describe the variations in the observed separation depth of DBZs, especially in older subducting plates.

## 5. Conclusions

[23] This study has used a reactive flow model to quantify the potential amounts of serpentinization that may occur in the mantle due to bending-related faulting prior to subduction. Although the estimated average chemically bound water content of hydrated mantle generally falls within the ranges predicted by prior observational studies, the model highlights the dependences of bend-fault serpentinization on plate age, subduction velocity and, most importantly, reaction kinetics. We show that the spacing of double Benioff zones is consistent with the temperature dependence of serpentine reaction kinetics. We also show that the observed seafloor temperature gradient in the bend-fault region is too low to be caused by 'one-pass' downward water flow into the serpentinizing lithosphere, but rather implies that bend-faults are areas of active hydrothermal flow, with the implied prediction that serpentine-sourced vents and chemosynthetic vent communities should be found in this deep-sea environment, too. This study also highlights the continuing need for new and improved coupled subduction zone models that integrate deformation, chemical reactions, and fluid flow to help further understand the causes and consequences of hydration and dehydration processes at subduction zones.

## Acknowledgments

[24] The authors would like to thank Manuele Faccenda and an anonymous reviewer for their constructive comments and criticisms which helped improve the paper.

## References

Andreani, M., A. Baronnet, A. M. Boullier, and J. P. Gratier (2004), A microstructural study of a "crack-seal" type serpentine vein using SEM and TEM techniques, *Eur. J. Mineral.*, *16*(4), 585–595, doi:10.1127/0935-1221/2004/0016-0585.

Angermann, D., J. Klotz, and C. Reigber (1999), Space-geodetic estimation of the Nazca-South America Euler vector, *Earth Planet. Sci. Lett.*, *171*(3), 329–334, doi:10.1016/S0012-821X(99)00173-9.

Billen, M. I. (2009), Tectonics: Soaking slabs, *Nat. Geosci.*, *2*(11), 744–746, doi:10.1038/ngeo674.

Billen, M. I., and M. Gurnis (2005), Constraints on subducting plate strength within the Kermadec trench, *J. Geophys. Res.*, *110*, B05407, doi:10.1029/2004JB003308.

Brudzinski, M. R., C. H. Thurber, B. R. Hacker, and E. R. Engdahl (2007), Global prevalence of double Benioff zones, *Science*, *316*(5830), 1472–1474, doi:10.1126/science.1139204.

Carlson, R. L., and D. J. Miller (2003), Mantle wedge water contents estimated from seismic velocities in partially serpentinized peridotites, *Geophys. Res. Lett.*, *30*(5), 1250, doi:10.1029/2002GL016600.

Conrad, C. P., and B. H. Hager (1999), Effects of plate bending and fault strength at subduction zones on plate dynamics, *J. Geophys. Res.*, *104*(B8), 17,551–17,571, doi:10.1029/1999JB900149.

Contreras-Reyes, E., and A. Osses (2010), Lithospheric flexure modelling seaward of the Chile trench: Implications for oceanic plate weakening in the Trench Outer Rise region, *Geophys. J. Int.*, *182*(1), 97–112, doi:10.1111/j.1365-246X.2010.04629.x.

Contreras-Reyes, E., I. Grevemeyer, E. R. Flueh, M. Scherwath, and M. Heesemann (2007), Alteration of the subducting oceanic lithosphere at the southern central Chile trench–outer rise, *Geochem. Geophys. Geosyst.*, *8*, Q07003, doi:10.1029/2007GC001632.

Contreras-Reyes, E., I. Grevemeyer, A. B. Watts, E. R. Flueh, C. Peirce, S. Moeller, and C. Papenberg (2011), Deep seismic structure of the Tonga subduction zone: Implications for mantle hydration, tectonic erosion, and arc magmatism, *J. Geophys. Res.*, *116*, B10103, doi:10.1029/2011JB008434.

Coumou, D., T. Driesner, S. Geiger, C. A. Heinrich, and S. Matthai (2006), The dynamics of mid-ocean ridge hydrothermal systems: Splitting plumes and fluctuating vent temperatures, *Earth Planet. Sci. Lett.*, *245*(1–2), 218–231, doi:10.1016/j.epsl.2006.02.044.

Dabrowski, M., M. Krotkiewski, and D. W. Schmid (2008), MILAMIN: MATLAB-based finite element method solver for large problems, *Geochem. Geophys. Geosyst.*, *9*, Q04030, doi:10.1029/2007GC001719.

Deschamps, F., S. Guillot, M. Godard, M. Andreani, and K. Hattori (2011), Serpentinites act as sponges for fluid-mobile elements in abyssal and subduction zone environments, *Terra Nova*, *23*(3), 171–178, doi:10.1111/j.1365-3121.2011.00995.x.

Dobson, D. P., P. G. Meredith, and S. A. Boon (2002), Simulation of subduction zone seismicity by dehydration of serpentine, *Science*, *298*(5597), 1407–1410, doi:10.1126/science.1075390.

Emmanuel, S., and B. Berkowitz (2006), Suppression and stimulation of seafloor hydrothermal convection by exothermic mineral hydration, *Earth Planet. Sci. Lett.*, *243*(3–4), 657–668, doi:10.1016/j.epsl.2006.01.028.

Engdahl, E. R., and C. H. Scholz (1977), Double Benioff zone beneath central Aleutians: An unbending of lithosphere, *Geophys. Res. Lett.*, *4*(10), 473–476, doi:10.1029/GL004i010p00473.

Escartín, J., G. Hirth, and B. Evans (1997a), Nondilatant brittle deformation of serpentinites: Implications for Mohr-Coulomb theory and the strength of faults, *J. Geophys. Res.*, *102*(B2), 2897–2913, doi:10.1029/96JB02792.

Escartín, J., G. Hirth, and B. Evans (1997b), Effects of serpentinization on the lithospheric strength and the style of normal faulting at slow-spreading ridges, *Earth Planet. Sci. Lett.*, *151*(3–4), 181–189, doi:10.1016/S0012-821X(97)81847-X.

Escartín, J., G. Hirth, and B. Evans (2001), Strength of slightly serpentinized peridotites: Implications for the tectonics of oceanic lithosphere, *Geology*, *29*(11), 1023–1026, doi:10.1130/0091-7613(2001)029<1023:SOSSPI>2.0.CO;2.

Faccenda, M., T. V. Gerya, and L. Burlini (2009), Deep slab hydration induced by bending-related variations in tectonic pressure, *Nat. Geosci.*, *2*(11), 790–793, doi:10.1038/ngeo656.

Faccenda, M., T. V. Gerya, N. S. Mancktelow, and L. Moresi (2012), Fluid flow during slab unbending and dehydration: Implications for intermediate-depth seismicity, slab weakening and deep water recycling, *Geochem. Geophys. Geosyst.*, *13*, Q01010, doi:10.1029/2011GC003860.

Fisher, A. T. (2005), Marine hydrogeology: Recent accomplishments and future opportunities, *Hydrogeol. J.*, *13*(1), 69–97, doi:10.1007/s10040-004-0400-y.

Fruh-Green, G. L., D. S. Kelley, S. M. Bernasconi, J. A. Karson, K. A. Ludwig, D. A. Butterfield, C. Boschi, and G. Proskurowski (2003), 30,000 years of hydrothermal activity at the Lost City vent field, *Science*, *301*(5632), 495–498, doi:10.1126/science.1085582.

Goetze, C., and B. Evans (1979), Stress and temperature in the bending lithosphere as constrained by experimental rock mechanics, *Geophys. J. R. Astron. Soc.*, *59*(3), 463–478, doi:10.1111/j.1365-246X.1979.tb02567.x.

Grevemeyer, I., N. Kaul, J. L. Diaz-Naveas, H. W. Villinger, C. R. Ranero, and C. Reichert (2005), Heat flow and bending-related faulting at subduction trenches: Case studies offshore of Nicaragua and central Chile, *Earth Planet. Sci. Lett.*, *236*(1–2), 238–248, doi:10.1016/j.epsl.2005.04.048.

Grevemeyer, I., C. R. Ranero, E. R. Flueh, D. Klaschen, and J. Bialas (2007), Passive and active seismological study of bending-related faulting and mantle serpentinization at the Middle America trench, *Earth Planet. Sci. Lett.*, *258*(3–4), 528–542, doi:10.1016/j.epsl.2007.04.013.

Hacker, B. R., S. M. Peacock, G. A. Abers, and S. D. Holloway (2003), Subduction factory: 2. Are intermediate-depth earthquakes in subducting slabs linked to metamorphic dehydration reactions?, *J. Geophys. Res.*, *108*(B1), 2030, doi:10.1029/2001JB001129.

Hensen, C., K. Wallmann, M. Schmidt, C. R. Ranero, and E. Suess (2004), Fluid expulsion related to mud extrusion off Costa Rica—A window to the subducting slab, *Geology*, *32*(3), 201–204, doi:10.1130/G20119.1.

House, L. S., and K. H. Jacob (1982), Thermal-stresses in subducting lithosphere can explain double seismic zones, *Nature*, *295*(5850), 587–589, doi:10.1038/295587a0.

Ishikawa, T., and E. Nakamura (1994), Origin of the slab component in arc lavas from across-arc variation of B and Pb isotopes, *Nature*, *370*(6486), 205–208, doi:10.1038/370205a0.

Ivandic, M., I. Grevemeyer, A. Berhorst, E. R. Flueh, and K. McIntosh (2008), Impact of bending related faulting on the seismic properties of the incoming oceanic plate offshore of Nicaragua, *J. Geophys. Res.*, *113*, B05410, doi:10.1029/2007JB005291.

Iyer, K., and Y. Y. Podladchikov (2009), Transformation-induced jointing as a gauge for interfacial slip and rock strength, *Earth Planet. Sci. Lett.*, *280*(1–4), 159–166, doi:10.1016/j.epsl.2009.01.028.

Iyer, K., H. Austrheim, T. John, and B. Jamtveit (2008a), Serpentinization of the oceanic lithosphere and some geochemical consequences: Constraints from the Leka Ophiolite Complex, Norway, *Chem. Geol.*, *249*(1–2), 66–90, doi:10.1016/j.chemgeo.2007.12.005.

Iyer, K., B. Jamtveit, J. Mathiesen, A. Malthe-Sorenssen, and J. Feder (2008b), Reaction-assisted hierarchical fracturing during serpentinization, *Earth Planet. Sci. Lett.*, *267*(3–4), 503–516, doi:10.1016/j.epsl.2007.11.060.

Iyer, K., L. H. Rüpke, and J. P. Morgan (2010), Feedbacks between mantle hydration and hydrothermal convection at ocean spreading centers, *Earth Planet. Sci. Lett.*, *296*(1–2), 34–44, doi:10.1016/j.epsl.2010.04.037.

John, T., M. Scambelluri, M. Frische, J. D. Barnes, and W. Bach (2011), Dehydration of subducting serpentinite: Implications for halogen mobility in subduction zones and the deep halogen cycle, *Earth Planet. Sci. Lett.*, *308*(1–2), 65–76, doi:10.1016/j.epsl.2011.05.038.

Jung, H., H. W. Green, and L. F. Dobrzhinetskaya (2004), Intermediate-depth earthquake faulting by dehydration embrittlement with negative volume change, *Nature*, *428*(6982), 545–549, doi:10.1038/nature02412.

Karato, S., and P. Wu (1993), Rheology of the upper mantle: A synthesis, *Science*, *260*(5109), 771–778, doi:10.1126/science.260.5109.771.

Kerrick, D. M., and J. A. D. Connolly (2001), Metamorphic devolatilization of subducted oceanic metabasalts: Implications for seismicity, arc magmatism and volatile recycling, *Earth Planet. Sci. Lett.*, *189*(1–2), 19–29, doi:10.1016/S0012-821X(01)00347-8.

Kummer, T., and G. A. Spinelli (2009), Thermal effects of fluid circulation in the basement aquifer of subducting ocean crust, *J. Geophys. Res.*, *114*, B03104, doi:10.1029/2008JB006197.

Lefeldt, M., and I. Grevemeyer (2008), Centroid depth and mechanism of trench-outer rise earthquakes, *Geophys. J. Int.*, *172*(1), 240–251, doi:10.1111/j.1365-246X.2007.03616.x.

Lefeldt, M., I. Grevemeyer, J. Gossler, and J. Bialas (2009), Intraplate seismicity and related mantle hydration at the Nicaraguan trench outer rise, *Geophys. J. Int.*, *178*(2), 742–752, doi:10.1111/j.1365-246X.2009.04167.x.

Lefeldt, M., C. R. Ranero, and I. Grevemeyer (2012), Seismic evidence of tectonic control on the depth of water influx into incoming oceanic plates at subduction trenches, *Geochem. Geophys. Geosyst.*, *13*, Q05013, doi:10.1029/2012GC004043.

Macdonald, A. H., and W. S. Fyfe (1985), Rate of serpentinization in seafloor environments, *Tectonophysics*, *116*(1–2), 123–135, doi:10.1016/0040-1951(85)90225-2.

Malvoisin, B., F. Brunet, J. Carlut, S. Rouméjon, and M. Cannat (2012), Serpentinization of oceanic peridotites: 2. Kinetics and processes of San Carlos olivine hydrothermal alteration, *J. Geophys. Res.*, *117*, B04102, doi:10.1029/2011JB008842.

Martin, B., and W. S. Fyfe (1970), Some experimental and theoretical observations on the kinetics of hydration reactions with particular reference to serpentinization, *Chem. Geol.*, *6*, 185–202, doi:10.1016/0009-2541(70)90018-5.

McNutt, M. K., and H. W. Menard (1982), Constraints on yield strength in the oceanic lithosphere derived from observations

of flexure, *Geophys. J. R. Astron. Soc.*, *71*(2), 363–394, doi:10.1111/j.1365-246X.1982.tb05994.x.

Meade, C., and R. Jeanloz (1991), Deep-focus earthquakes and recycling of water into the Earth's mantle, *Science*, *252*(5002), 68–72, doi:10.1126/science.252.5002.68.

Morris, J. D., W. P. Leeman, and F. Tera (1990), The subducted component in island-arc lavas: Constraints from Be isotopes and B-Be systematics, *Nature*, *344*(6261), 31–36, doi:10.1038/344031a0.

Okamoto, A., Y. Ogasawara, Y. Ogawa, and N. Tsuchiya (2011), Progress of hydration reactions in olivine-$H_2O$ and orthopyroxenite-$H_2O$ systems at 250°C and vapor-saturated pressure, *Chem. Geol.*, *289*(3–4), 245–255, doi:10.1016/j.chemgeo.2011.08.007.

Parsons, B., and J. G. Sclater (1977), Analysis of variation of ocean-floor bathymetry and heat-flow with age, *J. Geophys. Res.*, *82*(5), 803–827, doi:10.1029/JB082i005p00803.

Peacock, S. M. (2001), Are the lower planes of double seismic zones caused by serpentine dehydration in subducting oceanic mantle?, *Geology*, *29*(4), 299–302, doi:10.1130/0091-7613(2001)029<0299:ATLPOD>2.0.CO;2.

Plank, T., and C. H. Langmuir (1998), The chemical composition of subducting sediment and its consequences for the crust and mantle, *Chem. Geol.*, *145*(3–4), 325–394, doi:10.1016/S0009-2541(97)00150-2.

Raleigh, C. B., and M. S. Paterson (1965), Experimental deformation of serpentinite and its tectonic implications, *J. Geophys. Res.*, *70*(16), 3965–3985, doi:10.1029/JZ070i016p03965.

Ranero, C. R., J. P. Morgan, K. McIntosh, and C. Reichert (2003), Bending-related faulting and mantle serpentinization at the Middle America trench, *Nature*, *425*(6956), 367–373, doi:10.1038/nature01961.

Rüpke, L. H., J. P. Morgan, M. Hort, and J. A. D. Connolly (2002), Are the regional variations in Central American arc lavas due to differing basaltic versus peridotitic slab sources of fluids?, *Geology*, *30*(11), 1035–1038, doi:10.1130/0091-7613(2002)030<1035:ATRVIC>2.0.CO;2.

Rüpke, L. H., J. P. Morgan, M. Hort, and J. A. D. Connolly (2004), Serpentine and the subduction zone water cycle, *Earth Planet. Sci. Lett.*, *223*(1–2), 17–34, doi:10.1016/j.epsl.2004.04.018.

Schmidt, M. W., and S. Poli (1998), Experimentally based water budgets for dehydrating slabs and consequences for arc magma generation, *Earth Planet. Sci. Lett.*, *163*(1–4), 361–379, doi:10.1016/S0012-821X(98)00142-3.

Seno, T., and Y. Yamanaka (1996), Double seismic zones, compressional deep trench-outer rise events, and superplumes, in *Subduction Top to Bottom*, *Geophys. Monogr. Ser.*, vol. 96, edited by E. Bebout et al., pp. 347–355, AGU, Washington, D. C., doi:10.1029/GM096p0347.

Skelton, A., R. Whitmarsh, F. Arghe, P. Crill, and H. Koyi (2005), Constraining the rate and extent of mantle serpentinization from seismic and petrological data: Implications for chemosynthesis and tectonic processes, *Geofluids*, *5*(3), 153–164, doi:10.1111/j.1468-8123.2005.00111.x.

Sleep, N. H. (1979), Double seismic zone in downgoing slabs and the viscosity of the mesosphere, *J. Geophys. Res.*, *84*(B9), 4565–4571, doi:10.1029/JB084iB09p04565.

Spinelli, G. A., and K. Wang (2008), Effects of fluid circulation in subducting crust on Nankai margin seismogenic zone temperatures, *Geology*, *36*(11), 887–890, doi:10.1130/G25145A.1.

Spinelli, G. A., and K. Wang (2009), Links between fluid circulation, temperature, and metamorphism in subducting slabs, *Geophys. Res. Lett.*, *36*, L13302, doi:10.1029/2009GL038706.

Stein, C. A., and S. Stein (1992), A model for the global variation in oceanic depth and heat-flow with lithospheric age, *Nature*, *359*(6391), 123–129, doi:10.1038/359123a0.

Theissen-Krah, S., K. Iyer, L. H. Rüpke, and J. P. Morgan (2011), Coupled mechanical and hydrothermal modeling of crustal accretion at intermediate to fast spreading ridges, *Earth Planet. Sci. Lett.*, *311*(3–4), 275–286, doi:10.1016/j.epsl.2011.09.018.

Turcotte, D. L., and E. R. Oxburgh (1967), Finite amplitude convective cells and continental drift, *J. Fluid Mech.*, *28*, 29–42, doi:10.1017/S0022112067001880.

Turcotte, D. L., and G. Schubert (2002), *Geodynamics*, Cambridge Univ. Press, Cambridge, U. K.

Ulmer, P., and V. Trommsdorff (1995), Serpentine stability to mantle depths and subduction-related magmatism, *Science*, *268*(5212), 858–861, doi:10.1126/science.268.5212.858.

van Avendonk, H. J. A., W. S. Holbrook, D. Lizarralde, and P. Denyer (2011), Structure and serpentinization of the subducting Cocos plate offshore Nicaragua and Costa Rica, *Geochem. Geophys. Geosyst.*, *12*, Q06009, doi:10.1029/2011GC003592.

van Keken, P. E., B. R. Hacker, E. M. Syracuse, and G. A. Abers (2011), Subduction factory: 4. Depth-dependent flux of $H_2O$ from subducting slabs worldwide, *J. Geophys. Res.*, *116*, B01401, doi:10.1029/2010JB007922.

Wallmann, K. (2001), The geological water cycle and the evolution of marine delta O-18 values, *Geochim. Cosmochim. Acta*, *65*(15), 2469–2485, doi:10.1016/S0016-7037(01)00603-2.

Wegner, W. W., and W. G. Ernst (1983), Experimentally determined hydration and dehydration reaction rates in the system $MgO$-$SiO_2$–$H_2O$, *Am. J. Sci.*, *283-A*, 151–180.